University of Groningen

Polymer-wrapped carbon nanotubes for high performance field effect transistors

Derenskyi, Volodymyr

IMPORTANT NOTE: You are advised to consult the publisher's version (publisher's PDF) if you wish to cite from it. Please check the document version below.

Document Version
Publisher's PDF, also known as Version of record

Publication date:
2017

Link to publication in University of Groningen/UMCG research database

Citation for published version (APA):
Derenskyi, V. (2017). *Polymer-wrapped carbon nanotubes for high performance field effect transistors*. [Thesis fully internal (DIV), University of Groningen]. University of Groningen.

Copyright
Other than for strictly personal use, it is not permitted to download or to forward/distribute the text or part of it without the consent of the author(s) and/or copyright holder(s), unless the work is under an open content license (like Creative Commons).

The publication may also be distributed here under the terms of Article 25fa of the Dutch Copyright Act, indicated by the “Taverne” license. More information can be found on the University of Groningen website: https://www.rug.nl/library/open-access/self-archiving-pure/taverne-amendment.

Take-down policy
If you believe that this document breaches copyright please contact us providing details, and we will remove access to the work immediately and investigate your claim.

Downloaded from the University of Groningen/UMCG research database (Pure): http://www.rug.nl/research/portal. For technical reasons the number of authors shown on this cover page is limited to 10 maximum.

Download date: 02-02-2023

Chapter 4

Estimation of the purity of polymer-wrapped semiconducting SWNTs by single nanotube transistors fabrication

In this chapter we demonstrate short-channel ambipolar single-SWNT FETs prepared from a polymer-wrapped s-SWNT solution obtained with poly(2,5-dimethylidynenitrilo-3,4-didodecylthienylene) (PAMDD) polymer. No traces of metallic tubes were found in any of the prepared field effect transistors (646), implying an estimated purity of our semiconducting SWNT solution to be higher than 99.9%. These findings confirm the effectiveness of the polymer-wrapping technique in selecting semiconducting SWNTs, as well as the high quality of sorted nanotubes for the fabrication of not only nanotube network FETs, but also of short channel FETs using single or few nanotubes as active material.

V. Derenskyi, W. Gomulya, J. Gao, S. Z. Bisri, M. Pasini, Y.-L. Loo, M. A. Loi, submitted

4.1 Introduction

Following the discovery of the polymer-assisted SWNT selection method, polyfluorene-[1] and polythiophene-based[2] conjugated polymers with different side-chains[3] have demonstrated excellent ability to select semiconducting SWNTs based on their helicity and/or diameters. Indeed, s-SWNTs solutions prepared in this way have enabled the fabrication of high-performance SWNT network-based FETs exhibiting high on/off current ratio modulation (up to 10^8)[4], and charge mobility above 30 cm^2/ V·s.[3,5] However, the reported experimental results indicate that the high on/off ratio in network FETs is accompanied to relatively low mobilities (in the range of 5 cm^2/Vs),[4] while high mobilities are generally accompanied by on/off ratios equal or smaller than 10^6.[5–7] Generally, the decrease of the on/off ratio, or better, the measurement in FETs employing networks of SWNTs of off currents higher than the gate leakage current, has been attributed to the presence of metallic tubes in the channel. However, the use of transistor channel length often larger than the average length of the nanotubes and the relatively small differences in the off current, due to the high purity of the solutions, makes unreliable an evaluation of the purity based on the off current.

An estimation of the purity of semiconducting SWNTs solutions obtained by polymer wrapping using polyfluorene derivatives has been provided by evaluation of the on/off ratio of transistors of channel length of 240 nm using arrays of SWNTs.[8] In this work the authors estimate that on/off current of transistors above 10^3 are an indication that no metallic tubes are present in the channel. In another recent report, the purity of semiconducting arc-discharge nanotubes selected by using a polyfluorene derivative is estimated to be 98.3%, and is increased to above 99.9% by introducing an extra purification step.[9]

Recently we reported a very high semiconducting SWNT extraction yield by using the polymer poly(2,5-dimethylidynenitrilo-3,4-didodecylthienylene) (PAMDD),[5] which gave rise to network field effect transistors with mobility above 30 cm^2/Vs and on/off ratio of 10^6.

In this article, we aim at estimating the purity of semiconducting single-walled HiPCO carbon nanotubes obtained by polymer wrapping with PAMDD. Field effect transistors with channel length of 300 nm, i.e., smaller than the average length of the

SWNTs, were fabricated defining the electrodes by electron-beam lithography after deposition of the nanotubes sparsely on the gate dielectric. On/off current ratios as high as 10^5 for electron enhancement and 10^4 for hole enhancement regimes were obtained. In none of the measured devices short-circuits were observed. Such short-circuits would occur in short-channel SWNT-based FETs only if metallic SWNT species would be present in the channel. Given the absence of short-circuited devices, we estimate that the purity of the polymer-sorted s-SWNTs is higher than 99.9%.

4.2 Single-SWNT FETs characterization

s-SWNTs were selected with a polyazomethine (PAMDD)[10] polymer[5]. The chemical structure of PAMDD is shown in **Figure 1(a)**. The selection process consists of two main steps, ultrasonication and ultracentrifugation[11]. Briefly, the ultrasonication process destroys nanotube bundles, allowing the polymer to interact with the walls of SWNTs (Figure 1(b)) and to disperse individual nanotubes in organic solvents. During ultracentrifugation, the undispersed metallic nanotubes, bundles and other forms of carbon present in the as-synthesized material are removed. The excellent s-SWNT extraction yield obtained with PAMDD is attributed to the presence in the polymeric backbone of nitrogen (N) atoms, which display a very high affinity for the polarizable walls of SWNTs[14]. Moreover, the effect of the nitrogen atoms is combined with the presence of long alkyl side chains and the mechanical flexibility of the polymer backbone, all characteristics which together are favoring the selectivity for SWNTs and the high yield[5].

The absorption spectrum of the HiPCO-PAMDD solution is shown in Fig. 1(c). Two sets of sharp peaks in the ranges between 600 nm – 900 nm and 1000 nm – 1600 nm corresponding to the second (S_{22}) and the first (S_{11}) electronic transitions of s-SWNTs, respectively, are observed. The first electronic transitions of metallic nanotubes, M_{11}, usually appear in the range between 400 nm and 600 nm. However, in this case the broad absorption peak of PAMDD masks the relevant spectral region. This spectral overlap precludes the quantification of the purity of s-SWNTs by absorption spectroscopy. Therefore, an alternative method of evaluating the purity of s-SWNTs in the HiPCO-PAMDD solution is by analyzing the charge transport characteristics of the short-channel FETs, i.e., of devices with source-drain distance shorter than the average length of s-SWNTs (approx. 1 um)[11].

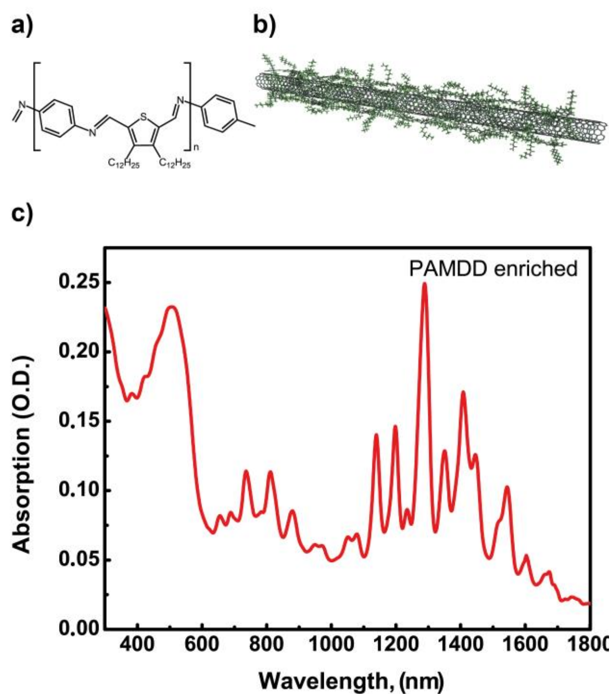

Figure 1. **(a)** Chemical structure of the PAMDD polymer used for the selection of the semiconducting SWNTs **(b)** schematic structure of a SWNT wrapped by a polymer chains **(c)** absorption spectra of the enriched HiPCO-PAMDD nanotube solution.

Figure 2(a) shows the optical micrograph of the fabricated devices with the central source electrode and 12 drain electrodes around it. The device structure schematic is illustrated in **Fig. 2(b)**. The distance between the electrodes is as short as 300 nm, as mentioned already a length chosen to avoid the formation of a SWNT network with nanotube-nanotube junctions within the transistor channel. In addition, the 300-nm channel width minimizes the probability of multiple SWNTs assembled in the channel region.

Using this configuration, we were able to study the performance of devices based on single or few s-SWNT bridging the source and drain electrodes.

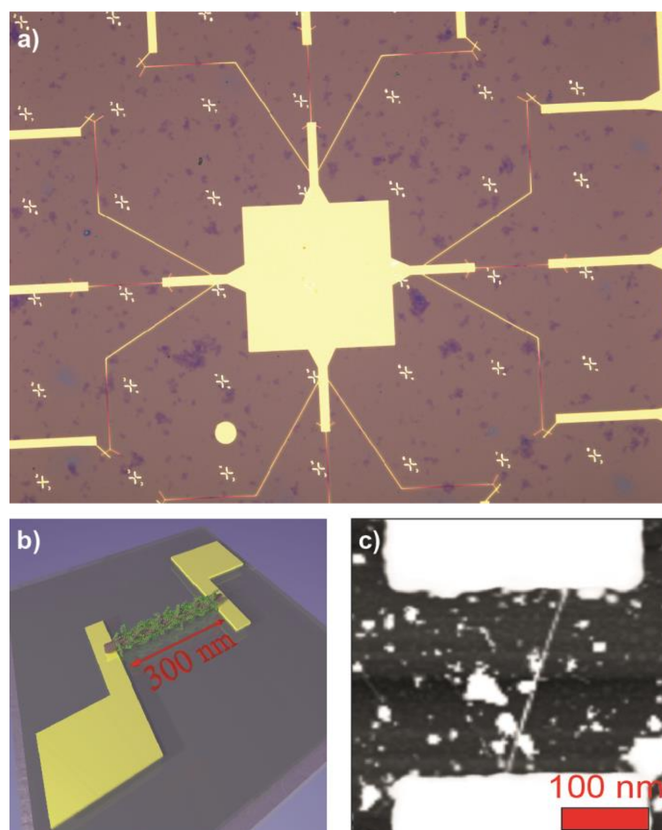

Figure 2. **(a)** Optical image of the fabricated FETs, one substrate includes 12 FETs with common source electrode in the center and drain electrodes at the edges. **(b)** Schematic structure of the single SWNT device. **(c)** AFM image of the source and drain electrodes forming the FET channel together with an individual SWNT. The channel width and length are 300 nm.

Two sets of SWNT FETs were fabricated for this experiment. HiPCO-PAMDD solutions with different s-SWNT concentrations were spin-coated on top of highly-doped Si wafer with thermally grown SiO_2. Top Ti/Au source and drain electrodes were subsequently defined by electron-beam lithography (Raith e-Line with a spatial resolution

of 6 nm). The experiment was repeated three times for each solution concentration for a total number of fabricated devices of 150 and 40 for the low and the high concentration solutions, respectively. Fig. 2(c) displays the atomic-force microscopy micrograph of a FET with an individual PAMDD-wrapped s-SWNT deposited between the electrodes, this sample was obtained with the low concentration solution. The white spots on the image are most probably due to residual polymer deriving from the polymer wrapping process and/or from the lithographic step.

The drain (V_D) and the gate (V_G) voltage dependences of the drain current are shown on **Fig. 3(a)** and **3(b)**, respectively. Out of 150 s-SWNT transistors measured, 46 exhibited semiconducting behavior and 104 FETs showed no drain current, due to the absence of nanotubes between the electrodes. This was verified by performing detailed AFM imaging in the channels of these devices. The relatively low yield of functional devices (31 %) is primarily due to the low probability of matching the randomly distributed SWNTs on the substrate with the top electrodes.

Because of the bottom-gate structure with conventional SiO_2 as gate dielectric, the devices were operated up to 60 V. Fig. 3(a) shows the I_D-V_D output characteristic of a single SWNT device; due to the short channel and the contact resistance, the output characteristics display a non-saturating behavior. The devices are ambipolar with the maximum hole current of about 0.2 μA and electron current around 25 nA. The transconductance curves showing values up to 8 nS are reported in the inset Fig. 3(c). These values are comparable with previously reported results on FETs made with a few polymer-wrapped SWNTs per channel[12], but because of the not-optimal gate dielectric they do not compete with the best devices reported recently using polymer wrapped SWNTs.[13] The current in the off-state (Fig. 3(b)) was as low as 5 pA and was limited by the resolution of the measurement set-up. The measured *on-* and *off*-currents in working transistors resulted in an average on/off ratio of 10^5 (Fig. 3(b)). Despite being limited by the applied drain voltage, these on/off ratio values are very high and comparable with the highest reported on/off ratios for solution-processed SWNT FETs with short transistor channel [12].

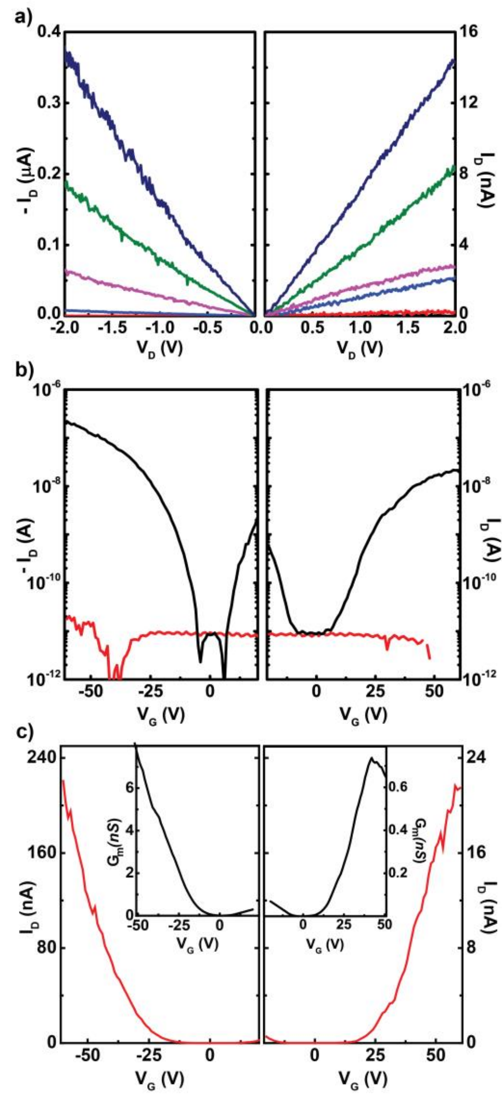

Figure 3. Electrical measurements of a single SWNT FET. **(a)** output I_D-V_D demonstrates gate-effect for V_G varying between 0 and 50 V (-50 V) with steps of 10 V (-10 V) **(b)** transfer I_D-V_D characteristics for p- and n-type channels measured in linear operational regime at $V_D = 0.4\ V$. Drain current (I_D, black curve) and Gate current (I_G, red curve) **(c)** transfer I_D-V_G characteristics in linear scale. Insets: Transconductance plot for single SWNT FET.

Unlike previous reports[14] showing that SWNT FETs with Ti/Au electrodes usually display unipolar p-type characteristics when fabricated in ambient conditions due to the trapping of electrons by adsorbed oxygen molecules,[15] our devices show ambipolar electrical behavior. Even though the device fabrication was also performed in ambient conditions, the annealing at 200^{0}C in nitrogen atmosphere for 2 h, allows removing the adsorbed oxygen[16–18] and to reestablish the intrinsic transport properties.

To increase the statistic on the nature of the SWNTs, we fabricated devices using more concentrated solution. **Fig. 4(a)** shows an AFM micrograph showing one of these transistors with several SWNTs between the electrodes. Fig. 4 (b) and (c) display representative I_D-V_D (output) and I_D-V_G (transfer) characteristics, respectively, obtained in a device comprising 10-15 s-SWNTs. Also in this case, transistors show higher p-type current, about 12 μA at (V_G=-50V and V_D =-2V), while the electron current (for V_G = 50 V and V_D = 2 V) is about 200 nA. The current appear to scale approximately with the number of the s-SWNTs bridging the channel. The Fig. 4(c) shows the transfer characteristics in linear regime, with measured on/off ratio values $>10^5$, demonstrating that all tubes within the channels are semiconducting. The inset Fig. 4(c) shows the transconductance of the same device.

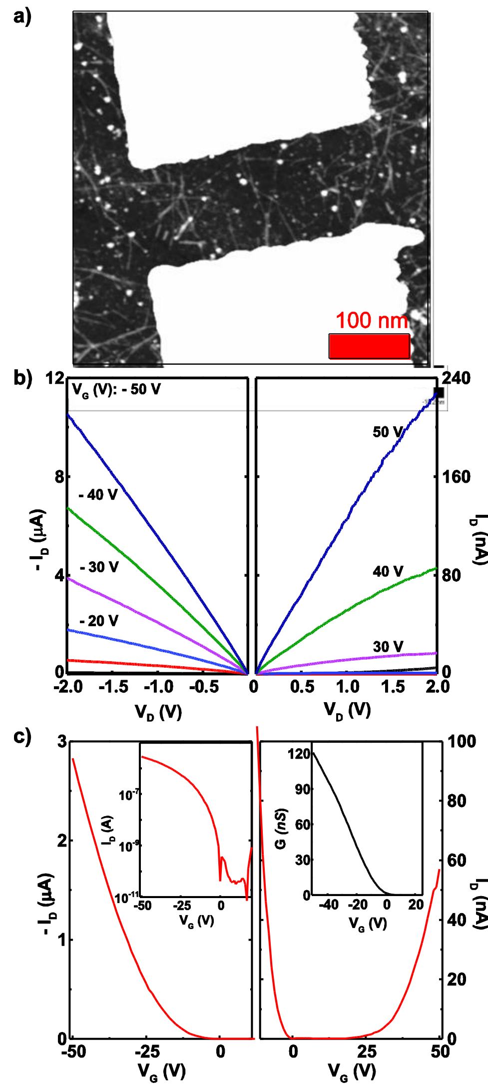

Figure 4. **(a)** AFM image of the channel region. **(b)** output characteristics ($|V_D| = 0.4$ V) of FETs with few SWNTs crossing the channel. Hole current in this FET demonstrates a 25 times increase compared to that in a single SWNT FET. **(c)** Linear scale of the transfer I_D-V_D characteristics for p- and n-type channels measured at $|V_D| = 0.4\ V$. Insets: Transfer characteristic in logarithmic scale (left) and conductance plot for multiple SWNT FET (right).

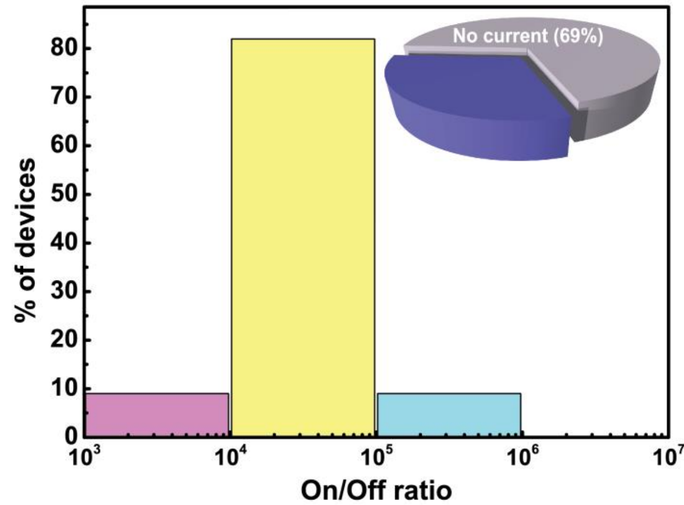

Figure 5. Diagram representing the distribution of on/off ratio in 150 FETs measured with single SWNT in the channel region. 69% of fabricated devices did not show any current due to the absence of SWNTs in channels. Working FETs demonstrated average on/off current ratio 10^5.

The diagram reported in **Fig.5** represents the statistical distribution of the on/off ratio of the fabricated transistors. 80% of working devices demonstrate an average on/off current ratio of 10^5 only about 9% show on/off between 10^4 and 10^3. Interestingly, of the 150 devices with single nanotubes and of the 40 devices with multiple tubes (an average of 15 tubes per device), for a total of 646 SWNTs measured, none of them showed the presence of metallic tubes. Therefore from these data we can estimate that the percentage of metallic tubes in our samples is lower that 0.1%, resulting in a purity for our semiconducting carbon nanotube solution > 99.9%. This value is underestimated; since no short-circuits where detected, a much larger number of devices would be required to precisely determine the purity of our s-SWNTs.

4.3 Conclusions

We have demonstrated short-channel ambipolar single-SWNT FET prepared from a polymer-wrapped s-SWNT solution. From 46 working single s-SWNT FETs and 40 multiple tubes (avg. 15 tubes) FETs, an average on/off current ratio of 10^5 is observed. No traces of metallic SWNTs were found in any of the prepared FETs (646 SWNTs tested), indicating an estimated purity of our semiconducting SWNT solution higher than 99.9%. These findings confirm the effectiveness of the polymer-wrapping technique in selecting semiconducting SWNTs, as well as the high quality of the sorted nanotubes for the fabrication of not only nanotube network FETs but also those comprising single and multiple nanotubes. In particular, the polyazomethine (PAMDD) is proven to be one of the best polymers for selecting semiconducting SWNTs with ultra-high purity, thanks to the interplay between the affinity for the nitrogen atoms of the highly polarizable walls of SWNTs and the mechanical flexibility of the polymeric backbone.

4.4 Experimental section

Preparation and characterization of the semiconducting SWNT dispersion: The polymer polyazomethine was dissolved in toluene with a concentration of 0.6 mg/mL, subsequently, 3 mg single-walled HiPCO (High Pressure Carbon Monoxide) carbon nanotubes (Unidym) were added. The solution was then sonicated with an Ultrasonic Liquid Processor (Sonicator 3000) for 2 hours at 65 W power and 16°C bath temperature. Two-step centrifugation using an ultracentrifuge (Beckman Coulter Optima XE-90; rotor: SW55Ti) was performed to remove bundles, carbon contaminants, and metallic nanotubes, as well as to enrich the SWNT solution.[14] During the first ultracentrifugation (1 h, 40000 rpm, 196000g), the high density components precipitated, forming a pellet at the bottom of the centrifugation tube, while the low density components containing individualized s-SWNTs wrapped by polymer remained in the upper part as supernatant. The second ultracentrifugation step (5 h, 55000 rpm, 367000g) was performed in order to enrich s-SWNTs and to remove any residual excess polymer[14]. Here, individualized s-SWNTs were precipitated to form a pellet. Finally, the pellet was re-dispersed in 2 mL of toluene to form ink for device fabrication.

The purity of the nanotube solution was examined by absorption spectroscopy using UV/Vis/NIR spectrophotometer (Shimadzu UV 3600). The spectra of the HiPCO nanotube solution were recorded in the range between 300 nm and 1800 nm.

Fabrication of carbon nanotube transistor: Highly doped silicon substrates with 300 nm thermally grown SiO_2 dielectric were used for FET fabrication. After cleaning the substrates[14], a solution of polymer-wrapped carbon nanotubes was spin-coated on top[13]. Spin-coating parameters (rotation speed, acceleration and duration) were chosen in such a way to form a SWNT film with the required density. The substrate was subsequently baked in a nitrogen atmosphere at 120℃ for 1 h to remove the residual organic solvent. The density was further analyzed by atomic force microscopy. The pattern was formed by electron beam lithography using positive polymer resist (polymethylmethacrylate [PMMA], Mw. = 950k), followed by a developing step in MIBK:IPA (methyl isobutyl ketone : isopropanol = 1:3) for 45 seconds. We then deposited 5 nm Ti adhesion layer and 25 nm Au source and drain electrodes using an electron beam evaporator (Temescal FC 2000). Finally, a lift-off procedure was performed in an ultrasonic acetone bath. Transistor channels formed in this way have 300 nm widths and 300 nm lengths. A schematic description of the transistor structure and fabrication process is shown in Fig. 2(b).

Characterization of the SWNT transistor: Electrical measurements were performed using a probe station placed in a nitrogen-filled glovebox at room temperature under dark conditions. The probe station was connected to Agilent E5262A Semiconductor Parameter Analyzer with a resolution of 5 pA. Because the fabrication process was performed in ambient conditions, the devices were annealed for 2 h at 200°C inside the glovebox to remove adsorbed water and oxygen molecules prior to measurements.

Characterization of SWNT networks by AFM: The SWNT within the channel of the FETs were imaged by AFM in tapping mode. The scanning region was the channel area exhibiting a size of 1 μm^2. The images were recorded with a MultiMode 6 Microscope and TESP probes (Bruker) with a spring constant k = 40 $N \cdot m^{-1}$, resonance frequency f = 40-75 kHz and an 8 nm tip radius. The scan rate and resolution of the measurements were selected to be 0.5 Hz and 1024 lines/sample, respectively. For each image, a new probe was employed in order to avoid AFM tip broadening due to wear of contamination from the conjugated polymer. The AFM images were analyzed using NanoScope Analysis software.

4.5 References

[1] W. Gomulya, G. D. Costanzo, E. J. F. de Carvalho, S. Z. Bisri, V. Derenskyi, M. Fritsch, N. Fröhlich, S. Allard, P. Gordiichuk, A. Herrmann, S. J. Marrink, M. C. dos Santos, U. Scherf, M. A. Loi, *Adv. Mater.* **2013**, *25*, 2948.

[2] H. W. Lee, Y. Yoon, S. Park, J. H. Oh, S. Hong, L. S. Liyanage, H. Wang, S. Morishita, N. Patil, Y. J. Park, J. J. Park, A. Spakowitz, G. Galli, F. Gygi, P. H.-S. Wong, J. B.-H. Tok, J. M. Kim, Z. Bao, *Nat. Commun.* **2011**, *2*, 541.

[3] S. P. Schießl, N. Fröhlich, M. Held, F. Gannott, M. Schweiger, M. Forster, U. Scherf, J. Zaumseil, *ACS Appl. Mater. Interfaces* **2015**, *7*, 682.

[4] V. Derenskyi, W. Gomulya, J. M. S. Rios, M. Fritsch, N. Fröhlich, S. Jung, S. Allard, S. Z. Bisri, P. Gordiichuk, A. Herrmann, U. Scherf, M. A. Loi, *Adv. Mater.* **2014**, *26*, 5969.

[5] W. Gomulya, V. Derenskyi, E. Kozma, M. Pasini, M. A. Loi, *Adv. Funct. Mater.* **2015**, n/a.

[6] N. Rouhi, D. Jain, K. Zand, P. J. Burke, *Adv. Mater.* **2011**, *23*, 94.

[7] N. Rouhi, D. Jain, P. J. Burke, *ACS Nano* **2011**, *5*, 8471.

[8] G. J. Brady, Y. Joo, M.-Y. Wu, M. J. Shea, P. Gopalan, M. S. Arnold, *ACS Nano* **2014**, DOI 10.1021/nn5048734.

[9] J. Ding, Z. Li, J. Lefebvre, F. Cheng, J. L. Dunford, P. R. L. Malenfant, J. Humes, J. Kroeger, *Nanoscale* **2015**, *7*, 15741.

[10] S. Destri, M. Pasini, C. Pelizzi, W. Porzio, G. Predieri, C. Vignali, *Macromolecules* **1999**, *32*, 353.

[11] S. Z. Bisri, J. Gao, V. Derenskyi, W. Gomulya, I. Iezhokin, P. Gordiichuk, A. Herrmann, M. A. Loi, *Adv. Mater.* **2012**, *24*, 6147.

[12] S. Park, H. W. Lee, H. Wang, S. Selvarasah, M. R. Dokmeci, Y. J. Park, S. N. Cha, J. M. Kim, Z. Bao, *ACS Nano* **2012**, *6*, 2487.

[13] G. J. Brady, A. J. Way, N. S. Safron, H. T. Evensen, P. Gopalan, M. S. Arnold, *Sci. Adv.* **2016**, *2*, e1601240.

[14] A. Javey, H. Kim, M. Brink, Q. Wang, A. Ural, J. Guo, P. McIntyre, P. McEuen, M. Lundstrom, H. Dai, *Nat. Mater.* **2002**, *1*, 241.

[15] V. Derycke, R. Martel, J. Appenzeller, P. Avouris, *Appl. Phys. Lett.* **2002**, *80*, 2773.

[16] A. Javey, J. Guo, D. B. Farmer, Q. Wang, E. Yenilmez, R. G. Gordon, M. Lundstrom, H. Dai, *Nano Lett.* **2004**, *4*, 1319.

[17] S. J. Wind, J. Appenzeller, R. Martel, V. Derycke, P. Avouris, *Appl. Phys. Lett.* **2002**, *80*, 3817.

[18] R. V. Seidel, A. P. Graham, J. Kretz, B. Rajasekharan, G. S. Duesberg, M. Liebau, E. Unger, F. Kreupl, W. Hoenlein, *Nano Lett.* **2005**, *5*, 147.